$$V(r,\varphi,\theta) = \frac{\mu}{r}\left\{1 + \sum_{n=2}^{N}\left(\frac{R}{r}\right)^n Y_n(\theta,\varphi)\right\}, \tag{1}$$

where μ is Earth's gravitational constant, r is the length of the radius vector from Earth's center of mass, R is the equatorial radius of the Earth, φ is the geocentric longitude and θ is the geocentric latitude. The spherical harmonic $Y_n(\varphi,\theta)$ is defined as

$$Y_n(\varphi,\theta) = \sum_{m=0}^{n} \bar{P}_n^m(\cos\theta)\left(\bar{C}_n^m \cos m\varphi + \bar{S}_n^m \sin m\varphi\right),$$

where $\{\bar{C}_n^0, \bar{C}_n^1, \ldots, \bar{C}_n^n, \bar{S}_n^1, \ldots, \bar{S}_n^n\}$ are normalized coefficients, and $\bar{P}_n^m$ are normalized associated Legendre functions of degree n and order m. As it is well known, V is a solution for the Laplace equation in spherical coordinates (r,φ,θ), $r > R$.

equ305D 1 T05D 0.905DaTD -e.423 Tc [(.A)4195982

The cost of evaluating V at a point (r,φ,θ)

Correlation matrices are dense because coefficients of the spherical harmonic expansion are not associated with any particular spatial location. Indeed, each coefficient in the expansion contributes to the field at every spatial location. Spherical harmonics are globally supported, oscillatory functions, which depend on cancellation (constructive interference) to achieve the approximation. Changing even a single coefficient in the model has a global effect. It is difficult, if not impossible, to adjust the spatial frequency content of a spherical harmonic expansion locally. In particular, there is a difficulty in incorporating observations of the gravitational potential near the surface with those obtained from satellites, which is due in part to the different spectral contents of the data.

Another important consideration is that the linear system for the L_2-minimization problem for model estimation has a very large condition number. Coupled with the global nature of spherical harmonic basis functions, this severely limits the overall resolution attainable in the model. We are unable to take advantage of the fact that measurements in some regions are better than in others, and the most poorly sampled region dictates the limit on the degree of resolution that can be attained globally.

Finally, computation of some satellite orbits appears to be very sensitive to the number of spherical harmonic terms retained in the model, and does not follow the common sense rule 'more terms are better.' It is indicative of an analogue of Gibbs' phenomenon since the magnitude of the normalized spherical harmonic model coefficients does not decrease significantly before the model is truncated. (Gibbs' phenomenon is a type of oscillatory error caused by abrupt truncation of a Fourier series with slowly decaying coefficients. A more detailed description is contained in Appendix B.)

Our goal is to develop multiresolution models of the Earth's gravity that do not suffer from the difficulties of estimation and evaluation outlined above. Multiresolution models use basis functions with localized support in both space and spectral domains. This allows us to generate models where changes in *most* of the parameters (coefficients) will produce only *local* changes in the model (up to any finite but arbitrary accuracy).

for estimation of the model parameters. Such bases also allow us to address the problem of ill-conditioning in an adaptive manner.

The particular choice of basis is a crucial issue since it will be necessary to use several different algorithms in conjunction with the representation. A number of authors (e.g. [1]) have constructed wavelet-type bases that respect the topology of the sphere. Although there certainly is merit to such constructions, we find them to be somewhat cumbersome for our purposes. Our preference is to use a more direct approach, where we employ ‘general purpose’ functions such as splines,

We introduce a grid on each square which is equispaced in the variables x and y. However, the projection of this grid back onto the spherical surface suffers a severe distortion due to stretching near the poles, since adjacent grid points become closer together the nearer they are to the poles. This gives rise to the pole problem mentioned above.

Using locally supported B-splines, we construct a representation of the geopotential on each shell, which interpolates the geopotential at each point of the grid.

Let r_i be a fixed distance from the center of the Earth which corresponds to the location of one of the concentric shells. The function S_i that describes the geopotential on the shell is defined by

$$S_i(x, y) = V(ta$$

where M is the order of the B-spline $\beta(x)$, and where $a(\xi)$ is defined by

$$a(\xi) = \sum_{1-M/2}^{M/2-1} \beta(k)\, e^{ik\xi}\,.$$

- Apply the inverse two-dimensional FFT to the matrix $\{\hat{s}^{n-1}_{i,j,k}\}$ to obtain the coefficient matrix $\{s^{n-1}_{i,j,k}\}$ on the coarser scale.

We note that multiresolution decomposition can be used in conjunction with any of the models described here, not just the doubly-periodic model.

The decomposition algorithm provides a simple and robust method for filtering the high frequency content of the model – high and low frequency can be extracted and represented separately. For example, Figure 1 in Appendix A illustrates how multiresolution decomposition is used to represent the low frequency portion of the field.

Such decomposition can be useful for the purpose of localizing the high frequency contribution of the gravity field. The need for such decomposition is apparent, see for example [2] or [3]. In [3] a deterministic modification of Stokes kernel is constructed for this purpose, with the goal of applying the results to computation of a gravimetric geoid. We feel that the models presented here, especially when coupled with the decomposition algorithm, might be useful in addressing such problems.

2.2. MULTIWAVELET CUBE MODEL

In this model, the surface of the sphere is mapped to the surface of a cube. Thus, the concentric shells form a sequence of nested cubes. A point on the surface of a sphere is mapped to a point on the reference cube (which has faces perpendicular to the coordinate axes and at a distance of one unit from the origin) using the following simple algorithm:

- Input coordinates (r, φ, θ) on the spherical surface of radius r.
- Compute $(x = r\sin\theta\cos\varphi,\ y = r\sin\theta\sin\varphi,\ z = r\cos\theta)$.
- Find $d = \max\{|x|, |y|, |z|\}$.
- Coordinates on the reference cube are $(\xi, \eta, \zeta) = (x/d, y/d, z/d)$.

Geometrically, we can think of a ray that emanates from the origin and intersects the sphere and the reference cube each in a single point. These two points are then mapped one to the other. (Mappings between cubic and spherical surfaces have been considered by other authors as well, see e.g. [4].)

The rectangular grid partitions each face of the cube into a number of square subdivisions, and we build a wavelet representation of the geopotential on each

TABLE I
Subdivision of the spherical surface to obtain six panels

Panel	Angle ranges	x-coordinate	y-coordinate
1	$-\pi \leqslant \varphi < -\pi/2, \quad -\pi/4 \leqslant \theta \leqslant \pi/4$	$\alpha\varphi + 3$	$\alpha\theta$
2	$-\pi/2 \leqslant \varphi < 0, \quad -\pi/4 \leqslant \theta \leqslant \pi/4$	$\alpha\varphi + 1$	$\alpha\theta$
3	$0 \leqslant \varphi < \pi/2, \quad -\pi/4 \leqslant \theta \leqslant \pi/4$	$\alpha\varphi - 1$	$\alpha\theta$
4	$\pi/2 \leqslant \varphi < \pi, \quad -\pi/4 \leqslant \theta \leqslant \pi/4$	$\alpha\varphi - 3$	$\alpha\theta$
5	$\lvert\gamma\rvert \leqslant 1, \lvert\omega\rvert \geqslant 1, \theta > 0$	$\alpha \tan^{-1}(\omega) \pm 2$	$-\alpha \sin^{-1}(\gamma)$
6	$\lvert\gamma\rvert \leqslant 1, \lvert\omega\rvert \geqslant 1, \theta < 0$	$\alpha \tan^{-1}(\omega) \pm 2$	$-\alpha \sin^{-1}(\gamma)$

ordinates (φ, θ) for each panel appear in the second column. Canonical coordinates on the face of each panel are (x, y), where $-1 \leqslant x, y \leqslant 1$, and these are obtained as indicated in columns 3 and 4 of the table with $\alpha = 4/\pi$. Panels designated 5 and 6 contain the north and south poles, respectively, and we define $\omega = \tan\theta / \cos\varphi$ and $\gamma = \cos\theta \sin\varphi$ in rows 5 and 6 of the table. For the x-coordinate in rows 5 and 6, we use the minus sign if $\omega > 0$ and the plus sign if $\omega < 0$.

We note that the B-spline expansion for each panel overlaps its immediate neighbors. Thus, to use this model for the estimation problem, we would need to add a certain number of equations to ensure that the representation near the boundaries of each panel is consistent with that of its neighbors.

2.3.2.

TABLE II
Size of local models

Order of model	Size in Mbytes
18	10.29
41	27.86
70	70.28

TABLE III
Comparison of evaluation times

Order of model	Time for sph. harm	Time for local model	Speed-up factor	Largest l_2 error
18	3.2745	0.8988	3.6430	0.12e-12
41	16.427	0.8410	19.532	0.16e-11
70	47.547	0.8471	56.130	0.13e-10

substantially more memory than spherical harmonic models. However, modern computers have sufficient RAM to handle the increased size easily.

Tests for timing and accuracy reported in Table III were done by comparing performance of the local model directly to the WGS84 spherical harmonic model [7]. The test consists of computing gravity vectors for 10,000 randomly generated points, then comparing execution times and accuracy. Accuracy is measured by computing the l_2-norm of the difference between the gravity vectors produced by the two different models, and reporting the largest error. Execution times are in seconds, and the speed-up factor is obtained by dividing the execution time for the spherical harmonic model by the execution time for the local model.

Observe that, while evaluation time for the spherical harmonic model increases

L^2-norm. In practice, the problem of finding u is often replaced by the problem of finding the corrections for u.

The actual estimation problem is more complicated since the input data often consists of measurements made from satellites, which contain errors due to various sources and, thus, at best can only be expected to be close to values of the actual geopotential. This situation brings in additional complications which we would like to ignore for now and, therefore, we confine our discussion to the problem of harmonic interpolation in order to illustrate several important points.

A traditional approach for solving the problem is to represent u with spherical harmonics and estimate the coefficients. We could thus make use of expression (1), which contains spherical harmonics up through degree and order N. This representation obviously solves the Laplace equation, and the problem is one of computing the coefficients to solve the interpolation problem (7). Difficulties occur

The definitions of $t_{k,l}^{n,p}$, $\beta_{k,l}^{j,p}$ and $\gamma_{k,l}^{j,p}$ are similar, and are obtained by substituting (9) into (8) and comparing the result to (10).

Collecting all such equations, for p

Acknowledgements

We gratefully acknowledge the invaluable contributions made to this work by Dr. Joseph Liu, who was instrumental in putting this program in motion, and also by Mark Storz, both of USAFSC. G. Beylkin; This research was partially supported by DARPA/AFOSR Grant DOD F49620-97-1-0017, DARPA/AFOSR Grant DOD F49620-98-1-0491 and DARPA/NASA Grant S43 5-28646. R. Cramer; This research was partially supported by DARPA/AFOSR Grant DOD F49620-97-1-0017 and DARPA/AFOSR Grant DOD F49620-98-1-0491.

Appendix A. Illustration of the Multiresolution Decomposition

In Figure 1 we illustrate the multiresolution decomposition of the geopotential (see §2.1.4) within the B-spline model. The underlying spherical harmonic model is EGM96 (360×360 order and degree model). The plot in the upper left corner is a high resolution display of a selected region of Earth's geopotential. This particular region was chosen because of the wide bandwidth of its features. Going from left to right and top to bottom, the sequence shows the successive coarsening using the multiresolution decomposition.

Appendix B. An Analogue of Gibbs' Phenomenon Due to Abrupt Truncation of the Spherical Harmonic Expansion

Let us present a comparison that illuminates diffculties inherent in current spherical harmonic models. We consider the difference between two models, WGS84-41 and WGS84-70 [7]. As the coefficients of WGS84-41 are identical with the coefficients of WGS84-70 up through order 41, we can view WGS84-41 as a truncated spherical harmonic expansion of the full WGS84-70 model. In the same way, WGS84-70 can be viewed as a truncation of even higher order models.

To illustrate our comparison, we plot the function V for both models WGS84-70 and WGS84-41 on the surface of the Earth aroud its equator, taking $r = R$, $\theta = \pi/2$, and $0 \leqslant \varphi \leqslant 2\pi$ in (1). This particular choice provides a good representative of the typical behavior.

Figure 2 shows the SGS84-70 model together with the WGS84-41 model and the difference between them. The relative difference is plotted in Figure 3.

The question that one might ask is what part of this difference is due to the analogue of Gibbs' phenomenon. (Gibbs' phenomenon is an oscillatory error which occurs if a Fourier series with slowly decaying coefficients is truncated abruptly. Here we refer to the abrupt truncation of the spherical harmonic expansion.) The difference between the two graphs is most likely due to the abrupt truncation. Spherical harmonics, being global, oscillatory functions, depend on cancellation

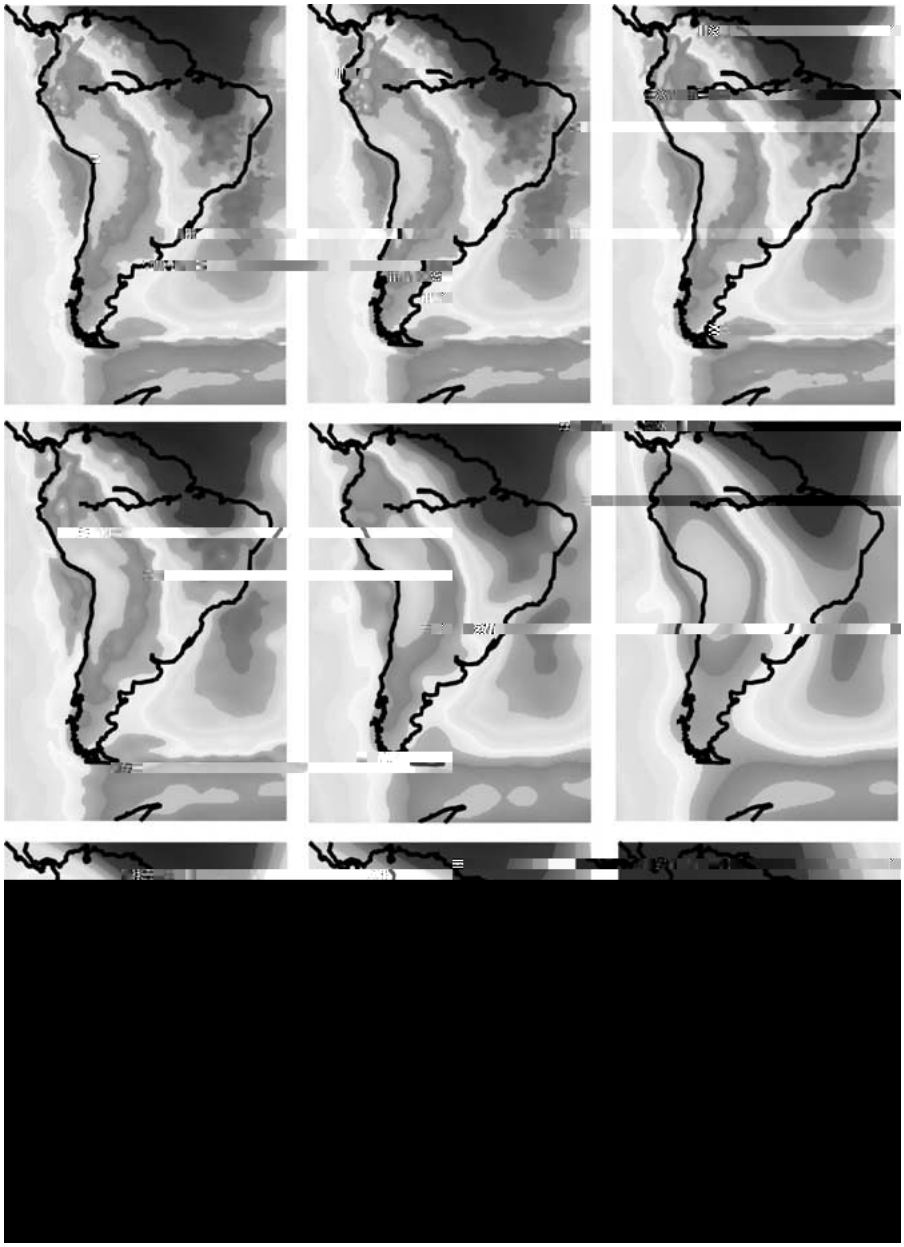

Figure 1. Multiresolution decomposition of a selected region using the B-spline representation of the spherical harmonic geopotential model EGM96.

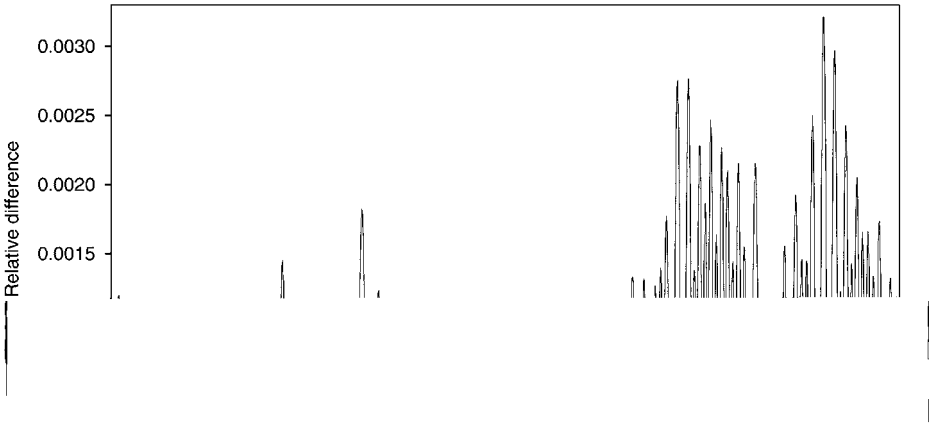

Figure 4. Relative difference between WGS84-70 and LWGS84-70R. Note that the difference is at most about 0.3%.

(destructive interference) to achieve the approximation. If high frequencies are removed by truncation then Gibbs' phenomenon occurs (in full analogy with Fourier series).

Now let us consider the B-spline approximation of the surface potential $V(r = R$ in (1)), obtained by interpolating V on an equispaced, two-dimensional grid. The size of the grid is roughly $4N \times 4N$, where N is the order and degree of the model, which is sufficient for a highly accurate representation of the potential function V (or its derivatives). For example, we use a 160×160 grid to represent the WGS84-41 model with accuracy $\approx 10^{-11}$ and represent the WGS84-70 model with the same accuracy on a 280×280 grid. Let us refer to the former B-spline representation as LWGS84-41 (local WGS84-41) and to the latter as LWGS84-70 (local WGS84-70). Model LWGS84-70 is, for practical purposes, indistinguishable from model WGS84-70, and LWGS84-41 is likewise indistinguishable from WGS84-41.

Performing one step of multiresolution decomposition (see §2.1.4) on the representation LWGS84-70, we obtain the reduced model, which we refer to as LWGS84-70R. This reduced model is supported on a 140×140 grid and thus is somewhat smaller in size than the LWGS84-41 model. The relative difference between LWGS84-70R and WGS84-70 is shown in Figure 4.

Note that the relative difference in Figure 4 is roughly 20 times smaller than that in Figure 3. This indicates a low information content of roughly half of the spherical harmonic coefficients in WGS84-70 model, corresponding to the high spatial frequencies. The B-spline model LWGS84-70R preserves the essential features of WGS84-70 much more faithfully than does WGS84-41, and yet it is practically devoid of high frequency content, and is essentially equivalent to WGS84-41 in its resolution. The difference is that LWGS84-70R was not obtained by an abrupt

truncation, but rather by a smoothing process which, unlike truncation, avoids the introduction of strong oscillatory artifacts (Gibbs' phenomenon).

In summary, we have seen that there exist significant differences between